DOI: 10.1002/ejic.200901190

Enthalpy/Entropy Compensation in the Melting of Thermotropic Nitrogen-Containing Chelating Ligands and Their Lanthanide Complexes: Successes and Failures

Aude Escande,[a][‡] Laure Guénée,[a] Emmanuel Terazzi,[a] Thomas B. Jensen,[a] Homayoun Nozary,[a] and Claude Piguet*[a]

Dedicated to Dr. Bertrand Donnio and Dr. Daniel Guillon[‡‡]

Keywords: Thermodynamics / Lanthanides / Liquid crystals / Thermotropic behavior / Polycatenar compounds

In this short overview dedicated to the thermodynamics of liquid crystalline chelating nitrogen-containing ligands and their lanthanide complexes (i.e., lanthanidomesogens), we first go through the initial successes obtained with the introduction of the concept of enthalpy/entropy compensation for rationalizing and programming melting and clearing temperatures in thermotropic mesophases. In the second part, the failures encountered during our attempts for switching from a qualitative toward a quantitative interpretation of the melting processes in polycatenar lanthanidomesogens are discussed, together with the delicate correlations established between the thermodynamic parameters of intermolecular cohesion measured in noncoordinating solvents and those operating in pure mesophases.

Introduction

When entering the field of metallomesogens (i.e., metal-containing liquid crystals),[1,2] the novice is surprised by the systematic and empirical approaches used for optimizing the temperature domain of existence of a thermotropic mesophase. In the vast majority of cases, the metals are embedded within some polyaromatic multidentate ligands to give neutral polarizable rigid cores, which are grafted with several flexible alkyl chains. Then, three strategies, which are often combined, can be recognized for designing thermotropic metallomesogens. (1) The length of the peripheral alkyl chains, together with the extension of the central rigid core are systematically varied to establish standard phase diagrams.[3] (2) Depending on the synthetic possibilities, various building units (O, S, CH_2, CF_2) are introduced within the peripheral flexible chains.[3,4] (3) The curvature of the molecular interface between the rigid core and the flexible part is stepwise modified by the connection of an increasing number of diverging alkyl chains.[5,6] Whereas thorough attention has been focused on the rationalization of the residual organizations detected in mesophases (nematic, lamellar, columnar, cubic) as a function of the variable molecular shapes and interface curvatures produced by these strategies,[7] the understanding and prediction of transition temperatures have been the subject of much less interest, despite their crucial role in the potential applications of thermotropic mesophases.[8] According to a very simple concept introduced by Skoulios and Guillon more than three decades ago,[9] the successive melting (crystal→mesophase) and clearing (mesophase→liquid) processes result from the microsegregation of a large amount of amphiphilic molecules, for which the minimum free energy is reached when like parts interact in a pairwise manner. Following this criteria, the polarizable metal-containing rigid cores are primarily associated by means of intermolecular interactions, whereas the less polarizable flexible alkyl chains fill the residual voids in the condensed phase (Figure 1).[10] Assuming, as a very rough approximation, a complete decorrelation between the intermolecular cohesion of the rigid cores and that of the flexible chains, this model predicts that the weak interchain enthalpic cohesion ($-\Delta H_m$) requires only a low temperature $T_m(\Delta G_m = 0) = \Delta H_m/\Delta S_m$ to be overcome by the considerable opposite entropic contribution ($T_m\Delta S_m$), a phenomenon usually referred to as the melting process, and which can be thought of in this context

[‡] Current address: Université de Rennes 1, Chimie Bâtiment B10A,
263 Av. Général Leclerc, 35042 Rennes, France
[‡‡]For their seminal contributions to the field of metal-containing liquid crystals.
[a] Department of Inorganic, Analytical and Applied Chemistry, University of Geneva,
30 quai E. Ansermet, 1211 Geneva 4, Switzerland
Fax: +41-22-379-6830
E-mail: Claude.Piguet@unige.ch
Supporting information for this article is available on the WWW under http://dx.doi.org/10.1002/ejic.200901190.

as the dispersion of correlated clusters of rigid cores in the continuum of the molten alkyl chains. A further increase of the temperature leads to a second compensation effect that occurs at $T_c(\Delta G_c = 0) = \Delta H_c/\Delta S_c$, when the stronger enthalpic cohesion between the rigid core ($-\Delta H_c$) is overcome by the weak opposite entropic contribution ($T_c\Delta S_c$). The latter transition is called the clearing temperature, because the semiorganized mesophase transforms into an isotropic liquid.

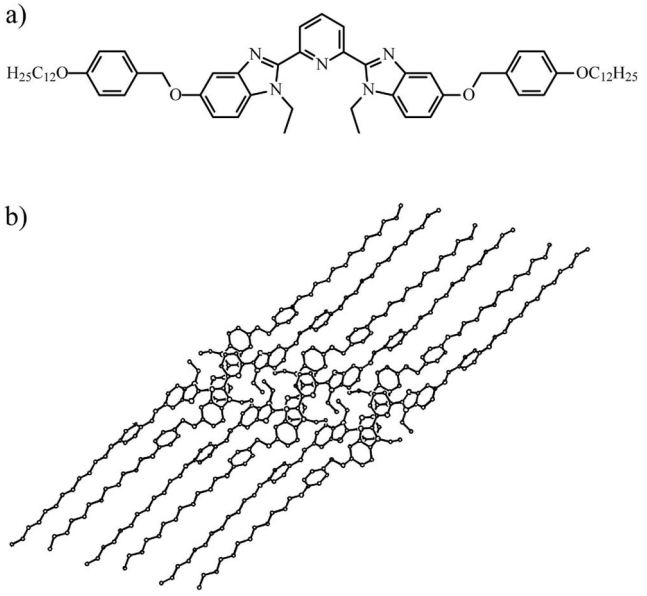

Figure 1. (a) An amphiphilic tridentate ligand and (b) its microsegregated organization in the crystalline state.[10]

Clearly, these two phenomena are not independent in real systems and some loss of cohesion between the rigid cores already occurs at the melting temperature T_m, which explains, for instance, the fluidity of mesophases. However, this two-step model allows for some pertinent comparisons between the melting of thermotropic liquid crystals that contain amphiphilic molecules, and that of simple hydrocarbons, for which detailed thermodynamic studies and rationalizations are available.[11] Williams and co-workers have demonstrated that the reduction of the intermolecular interactions between the alkyl chains occurring at the melting temperature for hydrocarbons indeed produces a change in dynamic between the two states (measured by $\Delta S_m > 0$), which is correlated with the reduction in bonding that accompanies the melting process ($\Delta H_m > 0$).[11] For pure hydrocarbon chains, incremental enthalpic ($\Delta H_{ass}^{incr} = -4$ kJ mol^{-1})[12] and entropic ($1.6 \leq -T\Delta S_{ass}^{incr} \leq 3.6$ kJ mol^{-1} at 298 K)[11b] contributions per methylene unit have been proposed. Consequently, once the branching of the alkyl chains is defined, the melting temperatures are found to be rather insensitive to the chain lengths [Equation (1)], a deduction often referred to as enthalpy/entropy compensation.[11,12]

$$T_m = \frac{\Delta H_m}{\Delta S_m} \simeq \frac{-\sum_n \Delta H_{ass}^{incr}}{-\sum_n \Delta S_{ass}^{incr}} = \frac{-n\Delta H_{ass}^{incr}}{-n\Delta S_{ass}^{incr}} = \frac{\Delta H_{ass}^{incr}}{\Delta S_{ass}^{incr}} \qquad (1)$$

Building on this reasoning, Ford has proposed a simple model for weak intermolecular association ($\Delta G_{ass} = \Delta H_{ass} - T\Delta S_{ass}$) between two molecules, which implies that ΔH_{ass} depends on the minimum of the binding potential [u_{min} in Equation (2), k_b is Boltzmann's constant], whereas ΔS_{ass} is related to the force constant of the interaction; κ in Equation (3), once the reference concentration ($1/V_{ref}$) is fixed.[13]

$$\Delta H_{ass} = u_{min} + \tfrac{3}{2} k_b T \qquad (2)$$

$$\Delta S_{ass} = k_b \ln\left(\frac{(2\pi e)^{3/2}}{V_{ref}}\right) - \tfrac{3}{2} k_b \ln\left(\frac{\kappa}{k_b T}\right) \qquad (3)$$

When a perturbation is imposed upon the pair of associated molecules, for instance, the stepwise increase in length of the flexible chains previously discussed, the enthalpy/entropy compensation requires that u_{min} and κ move in the opposite direction, so that $|\Delta H_{ass}|$ and $|\Delta S_{ass}|$ both decrease or both increase. However, there is no fundamental principle of weak interaction that dictates the relative dependence of well depth u_{min} and force constant κ. Within the frame of a simple Lennard-Jones (12,6) potential $V = 4\varepsilon[(r_0/r)^{12} - (r_0/r)^6]$ for roughly modeling an intermolecular interaction,[14] the harmonic approximation applied to the minimum of the attractive well yields $u_{min} = -\varepsilon$ ($u_{min} < 0$) and $\kappa = 2\varepsilon/(r_0)^2$ ($\kappa > 0$), whereby r_0 is the intermolecular separation at which $V = 0$ (Figure 2).[13,14] Combining these results with Equations (2) and (3) predicts that compensation only occurs under conditions in which ε varies and r_0 is fixed, a situation that is apparently found for the intermolecular cohesion between hydrocarbons of increasing length,[11,12] but that has no obvious reason to be retained for other structural variations.[13]

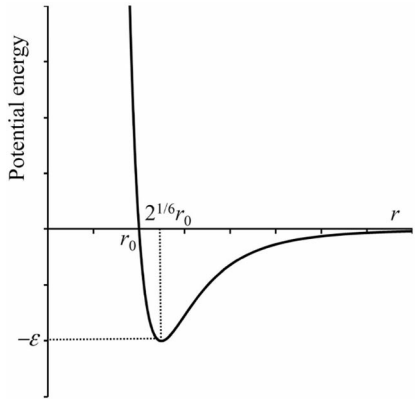

Figure 2. Representation of a Lennard-Jones (12,6) potential $V = 4\varepsilon[(r_0/r)^{12} - (r_0/r)^6]$ with the interpretation of ε and r_0 parameters.

Based on this approach, we suspect that the systematic variation in length of the flexible chains usually investigated for establishing phase diagrams in thermotropic mesogens has little impact on the melting temperatures compared with more substantial perturbations, such as the grafting of several diverging flexible chains in polycatenars, polypeds, and dendrimers.[5–7] Moreover, detailed investigations of

ΔH_m and ΔS_m measured by differential scanning calorimetry (DSC) for first-order transitions in homologous series could give some insights into the structural and/or chemical programming of the molecular parameters ε and κ. Obviously, the same approach applies to clearing processes assuming that (i) the well depth $-\varepsilon$ corresponds to interaromatic stacking interactions[15] and (ii) the relaxation of the degrees of freedom (ΔS_c) is limited by the rigid character of the polyaromatic core.

Results and Discussion

Successful Manipulations of Melting and Clearing Processes in Nitrogen-Containing Chelating Ligands and Their Lanthanide Complexes

Since 2,2′-bipyridine is the archetype of nitrogen-containing chelating ligands in coordination chemistry, let's start with the thermal behaviors of homologous dicatenar (**L1**^{Cn}), tetracatenar (**L2**^{Cn}), and hexacatenar (**L3**^{Cn}) bipyridine ligands that possess alkyl chains with variable lengths (Figure 3).[16] The minor changes detected for the melting temperatures of the dicatenar bipyridines **L1**^{Cn} ($209 \leq T_m \leq 269$ °C for $1 \leq n \leq 14$, Figure 3, a) unambiguously demonstrate that enthalpy/entropy compensation (i.e., $\Delta H_m/\Delta S_m \approx$ constant) operates when the chain length is simply increased,[16] as reported for simple hydrocarbons.[11] A similar behavior is observed for the closely related dicatenar lipophilic ligands **L4**^{Cn}, in which the central bidentate bipyridine is replaced with a tridentate 2,6-bis(benzimidazol-2-yl)pyridine scaffold coded for trivalent lanthanides, Ln^{III} (Figure 4a, T_m = 187 °C for **L4**^{C6} and T_m = 206 °C for **L4**^{C12}).[17] The tetracatenar bipyridines **L2**^{Cn} also display a minor dependence of T_m (melting) and T_c (clearing) on increasing chain lengths (Figure 3, b, $T_m^{n=14}/T_m^{n=4} \approx T_c^{n=4}/T_m^{n=14} = 1.2$ for T in Kelvin), but the initial steeper decrease evidenced on going from $n = 4$ to $n = 8$ can be assigned to some partial unbalanced changes in entropies, in other words, to an increase of the force constant κ [Equation (3)], which is not overcome by a concomitant deepening of the potential. This trend is confirmed in the hexacatenar series **L3**^{Cn} (Figure 3, c), for which the effect of an increase in chain length significantly deviates from the expected entropy/enthalpy compensation effect ($T_m^{n=1}/T_m^{n=12} = 1.5$).[13] However, the latter trend remains minor compared with the striking decrease of T_m and T_c that results from the connection of an increasing number of divergent alkyl chains to the central rigid core. For $n = 8$ in Figure 3, we indeed observe T_m(**L1**^{C8}) = 231 °C > T_m(**L2**^{C8}) = 173 °C >> T_m(**L3**^{C8}) = 85 °C, which can be associated with a "polycatenar" effect whereby ε and r_0 are not correlated, a behavior fully compatible with Equations (2) and (3).[13]

Closely related decreases in melting temperature, which can be referred to as "polycatenar" effects, are observed on going from the dicatenar tridentate ligand **L5**^{C12} (T_m = 154 °C, ΔH_m = 63 kJ mol^{-1}, ΔS_m = 147 J mol^{-1} K^{-1}) to the tetracatenar analogue **L6**^{C12} (T_m = 74 °C, ΔH_m = 96 kJ mol^{-1}, ΔS_m = 276 J mol^{-1} K^{-1}, Figure 4, b),[18] or along the series depicted in Figure 4 (c) (**L7**^{C12}: dicatenar, T_m = 131 °C;[10] **L8**^{C12}: hexacatenar, T_m = 25 °C;[19] and **L9**^{C12}: dodecacatenar, T_m = –34 °C).[20] These observations suggest that a decrease in the melting temperature can be empirically correlated with an increase in the number of connected divergent alkyl chains, given that their length is sufficient (let's say $n \geq 6$) to produce microsegregation in the solid state. The same trend is observed for the lanthanidomesogens [Ln(**L*k***^{C12})(NO$_3$)$_3$] (***k*** = 4–9; Ln = La–Lu, except Pm) obtained with these ligands, except that the expansion of the rigid core brought by the Ln(NO$_3$)$_3$ unit produces adequate microsegregation and thermotropic mesophases only for the hexacatenar **L8**^{C12} and dodecatanar **L9**^{C12} ligands.[10,17–20] Although the size of the trivalent lanthanide significantly influences the melting temperature, the trend observed in the free ligand is retained in the complexes with T_m{[Ln(**L8**^{C12})(NO$_3$)$_3$]} = 70 to 160 °C (hexacatenar)[19] >> T_m{[Ln(**L9**^{C12})(NO$_3$)$_3$]} = –43 to –25 °C (dodecacatenar).[20] Following the same strategy, we approached the programming of clearing temperatures, T_c, by means of the tuning of interaromatic interactions based on variable polarizations of the aromatic rings.[15] Rowe and Bruce attempted to explore the effect of different alternation of polarization on the global permanent electric dipole of the molecule and its consequence on the thermal behavior of ligands **L1**^{C8} and **L10**^{C8}, but decomposition unfortunately occurred prior to isotropization (Figure 5, a).[16] Switching from bipyridine-based (**L1**^{C8} and **L10**^{C8}) to bis(benzimidazole)pyridine-based binding units in **L8**^{C12} and **L11**^{C2} provides experimentally accessible clearing temperatures (Figure 5, b).[21] The larger number of polarization inversions found along the strand in **L11**^{C12} (seven instead of five in **L8**^{C12}) indeed induces the expected,[15,22] stronger cohesion between the rigid aromatic groups [ΔH_c(**L11**^{C12}) = 4.0 kJ mol^{-1} compared with ΔH_c(**L8**^{C12}) = 3.3 kJ mol^{-1}].[21]

This polarization effect is further amplified upon coordination of the central tridentate binding unit to Lu^{3+} in [Lu(**L8**^{C12})(NO$_3$)$_3$] and [Lu(**L11**^{C12})(NO$_3$)$_3$], as exemplified by the molecular electrostatic potentials computed on the Connolly surface, which show that the complexed ligand strand in [Lu(**L11**^{C12})(NO$_3$)$_3$] now displays a smaller number of polarization inversions than [Lu(**L8**^{C12})(NO$_3$)$_3$] (Figure 6).[21] Consequently, the clearing temperature T_m{[Lu(**L11**^{C12})(NO$_3$)$_3$]} = 120 °C is significantly lower than that found for the parent complex T_m{[Lu(**L8**^{C12})(NO$_3$)$_3$]} > 223 °C.[23]

Failures in the Quantification of the Enthalpic and Entropic Contributions to Melting and Clearing Processes in Lanthanidomesogens

Severely criticized by reviewers and colleagues on several occasions, we decided to explore the possibility of finding some unambiguous quantitative demonstrations for the

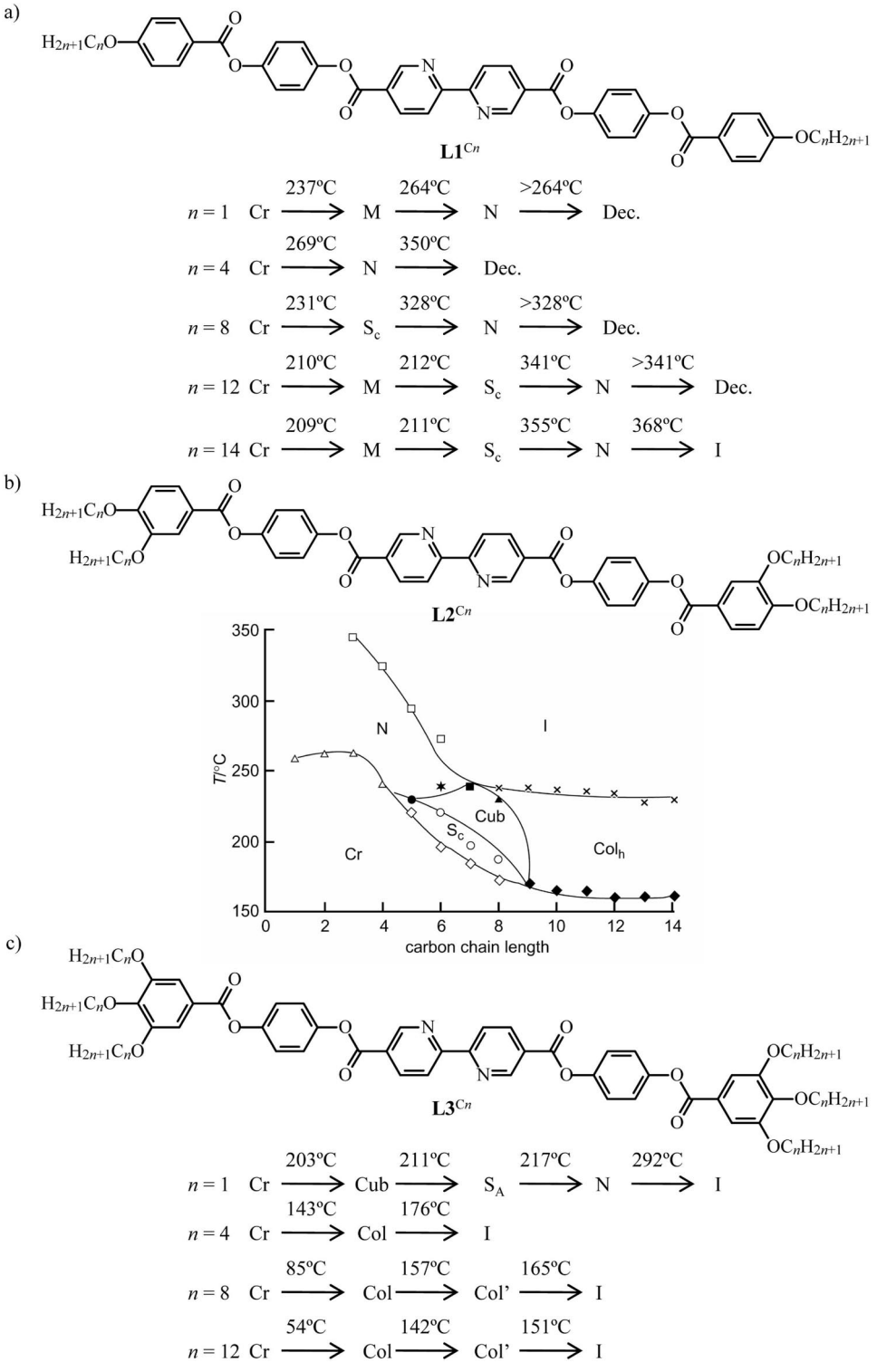

Figure 3. Thermal behaviors of (a) dicatenar, (b) tetracatenar, and (c) hexacatenar liquid crystals based on 2,2′-bipyridine (Cr = crystal, M = unknown mesophase, S_A = smectic A, S_C = smectic C, N = nematic, Cub = cubic, Col = columnar, I = isotropic liquid, Dec. = decomposition).[16]

prediction of ΔH_m and ΔS_m in a series of well-defined lanthanidomesogens. To maximize our chance of success, we focused on the 6,6′-disubstituted V-shaped ligands **L12**^{C12}, **L13**^{C12}, and **L14**^{C12} because the final formation of rodlike I-shape complexes [Ln(**L*k***^{C12})$(NO_3)_3$] favors close intermolecular approach (Scheme 1).[19] The syntheses of **L12**^{C12}–**L14**^{C12} follow a strategy in which the 2,6-bis[(2-ethyl-6-hydroxybenzimidazol)-2-yl]pyridine synthon is coupled with adequately substituted benzoic acid derivatives (Scheme S1 in the Supporting Information). The elemental analyses

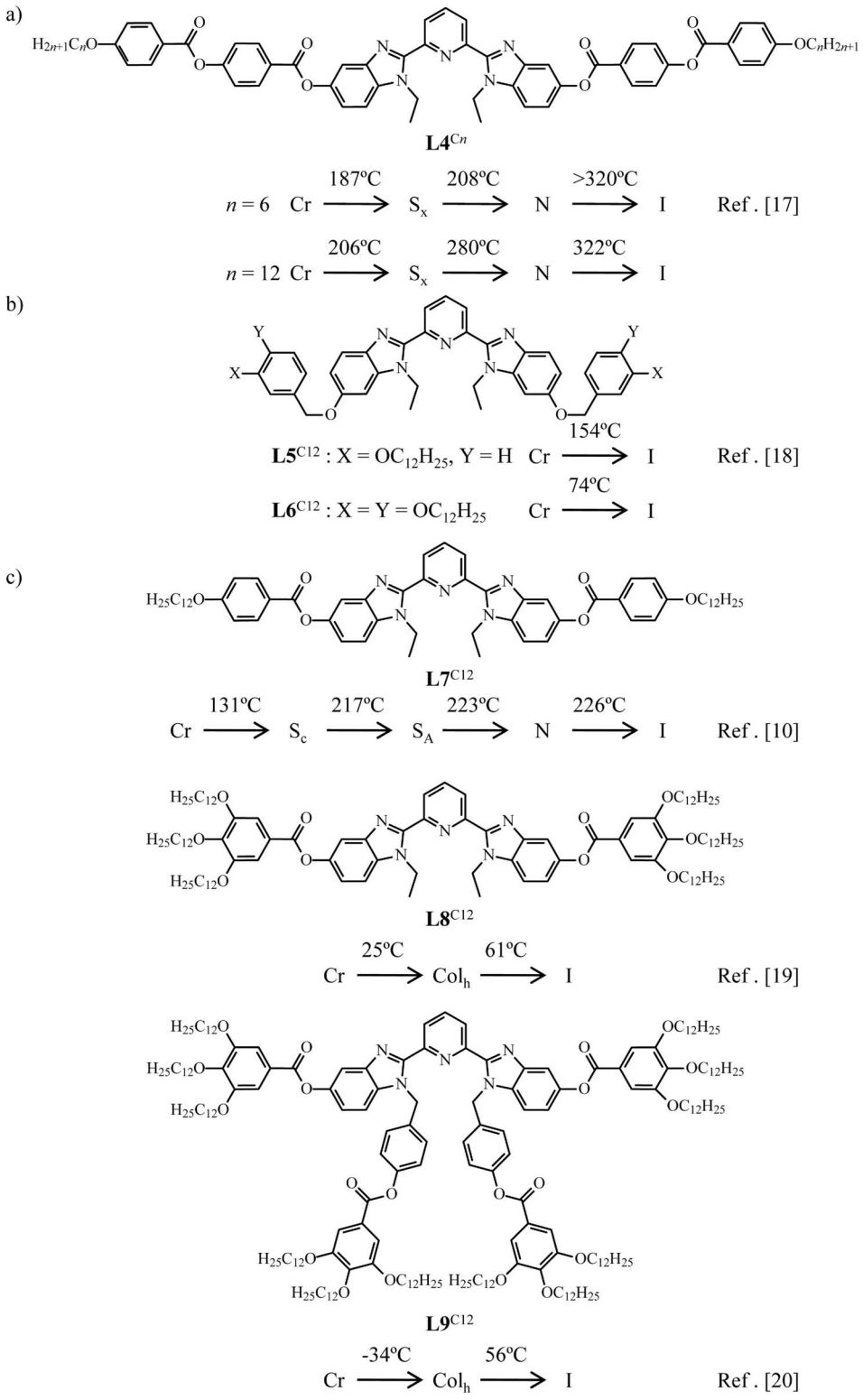

Figure 4. Thermal behaviors of three series of polycatenar liquid crystals based on 2,6-bis(benzimidazol-2-yl)pyridine (Cr = crystal, S_A = smectic A, S_C = smectic C, S_x = unknown smectic mesophase, N = nematic, Col_h = hexagonal columnar, I = isotropic liquid).

(Table S1 in the Supporting Information) confirm the purity of the ligands. The symmetry of the ^1H NMR spectrum (two equivalent benzimidazole rings, enantiotopic methylene protons, Figure 7, a), combined with the absence of any nuclear Overhauser enhancement effect (NOE) between the pyridine proton H^2 and the ethyl protons in the central tridentate binding unit, implies an average C_{2v}-symmetrical arrangement of the ligand strand, in which the nitrogen do-

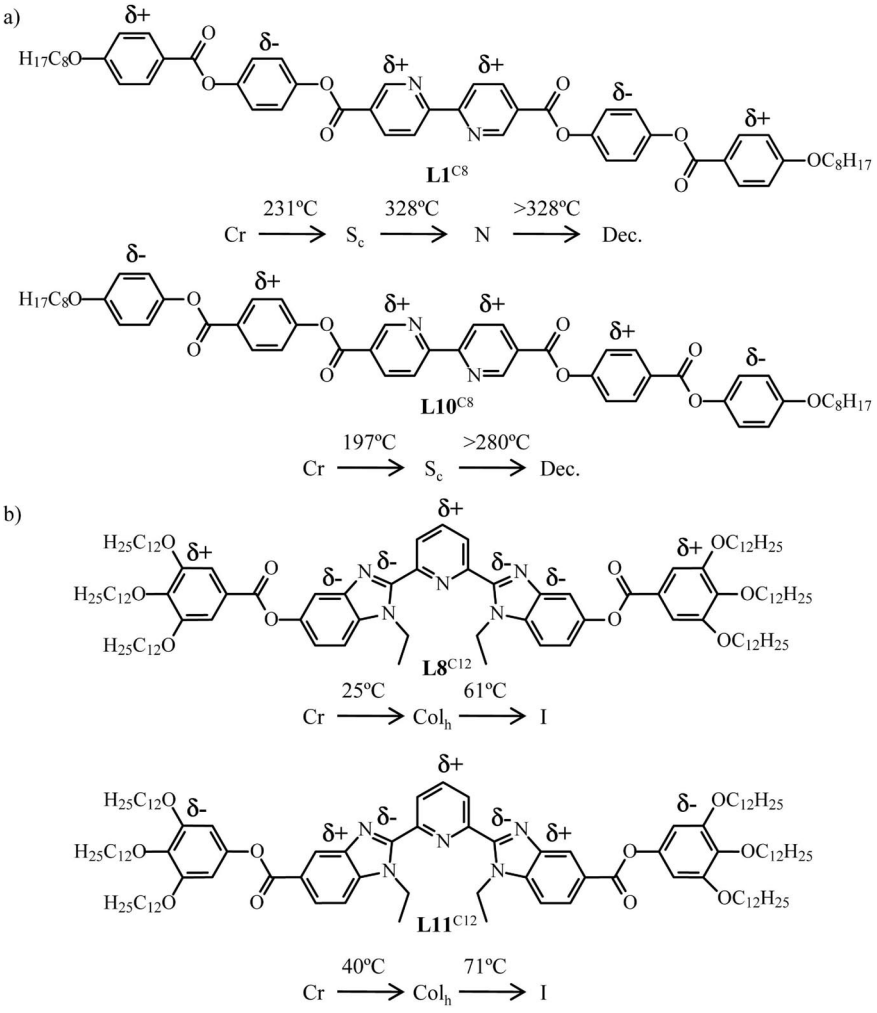

Figure 5. Thermal behaviors of two series of liquid crystalline ligands containing aromatic groups with alternated polarizations (Cr = crystal, S_C = smectic C, N = nematic, Col_h = hexagonal columnar, I = isotropic liquid, Dec. = decomposition).

nor atoms display a *trans,trans* conformation (Scheme 1, top).[10,17–20] The free ligands **L12**^{C12}–**L14**^{C12} simply melt to give isotropic liquids (first-order phase transitions, Table 1). We note an abrupt change in the melting temperature on going from the dicatenar ligand **L12**^{C12} (T_m = 172 °C) to the tetracatenar analogue **L13**^{C12} (T_m = 57 °C), which can be assigned to the 50% increase of ΔS_m. The connection of two additional dodecyloxy chains in the hexacatenar ligand **L14**^{C12} does not further significantly affect T_m (i.e., $T_m = \Delta H_m/\Delta S_m$ = constant), because both enthalpic and entropic contributions are reduced by the same 0.65 ratio (Table 1). Upon reaction of **L12**^{C12} or **L13**^{C12} with $Ln(NO_3)_3{\cdot}xH_2O$ (Ln = La, Eu, Lu, Y) in CH_2Cl_2/CH_3CN (1:1), pure [Ln(**L*k***^{C12})$(NO_3)_3$] complexes can be isolated in the solid state in fair to good yields (***k*** = 12, 13; Tables S1–S3), as previously established for [Ln(**L14**^{C12})$(NO_3)_3$] (Ln = Pr–Lu, except Pm).[19]

In contrast with the rich mesomorphism observed for the latter hexacatenar complexes (lamello-columnar, hexagonal columnar, and cubic organizations, Table 1), the lanthanide complexes with **L12**^{C12} and **L13**^{C12} only display complicated series of first-order crystal→crystal phase transitions [established by polarized light microscopy (PLM) and small-angle X-ray diffraction (SA-XRD) measurements] prior to undergoing decomposition at high temperature (>200 °C). This disappointing result prevents us from quantitatively addressing possible variations of ΔH_m and ΔS_m with (i) an increasing number of diverging dodecyloxy chains and (ii) the variable size of the central metal in lanthanidomesogens. However, it is clear that the temperature of the melting process in the complexes is higher than decomposition (>200 °C) for the complexes with dicatenar (**L12**^{C12}) and tetracatenar (**L13**^{C12}) ligands, whereas significantly lower values are found for the hexacatenar analogues (T_m{[Ln(**L14**^{C12})$(NO_3)_3$]} = 100–160 °C, Table 1). We thus conclude that the major unbalanced enthalpy/entropy change, which is responsible for the beneficial polycatenar effect, indeed occurs between dicatenar and tetracatenar series in the free ligands (quantitatively supported in Table 1), whereas it is unfortunately shifted between tetra-

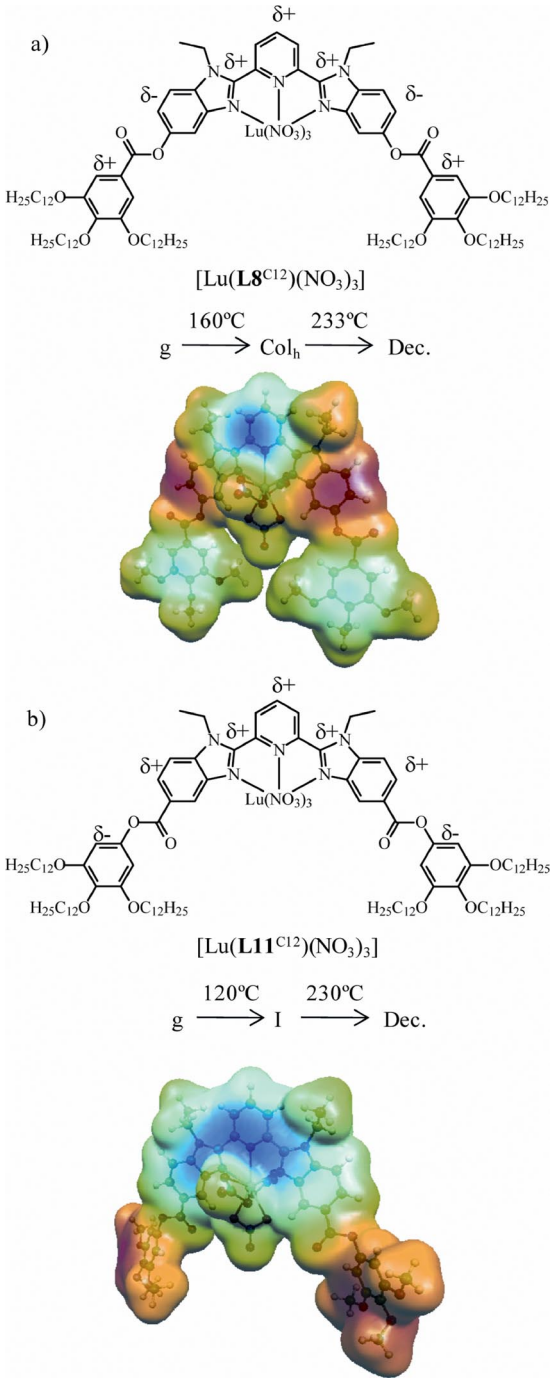

Figure 6. Schematic structures and polarizations, and associated color-coded representation of DFT molecular electrostatic potentials (MEP) computed on the Connolly surfaces around (a) $[Lu(\mathbf{L8}^{C1})(NO_3)_3]$ and (b) $[Lu(\mathbf{L11}^{C1})(NO_3)_3]$ in their optimized gas-phase geometries (blue = electron-deficient domain, red = electron-rich domain; g = glassy state, Col_h = hexagonal columnar, I = isotropic liquid, Dec. = decomposition). Adapted from ref.[21]

and hexacatenar units in the associated lanthanidomesogens, thus preventing its stepwise quantitative exploration along the series $[Ln(\mathbf{L}\boldsymbol{k}^{C12})(NO_3)_3]$ ($\boldsymbol{k}$ = 12–14).

However, can we find an alternative method for assigning the abrupt changes in the thermal behaviors along the series

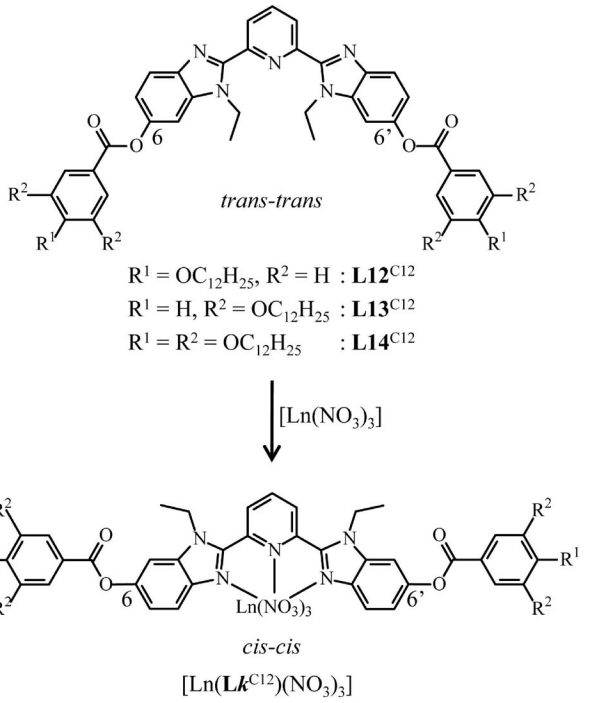

Scheme 1. Chemical structures of the polycatenar V-shape ligands $\mathbf{L12}^{C12}$–$\mathbf{L14}^{C12}$ and formation of the associated I-shape complexes $[Ln(\mathbf{L}\boldsymbol{k})(NO_3)_3]$.

of complexes $[Ln(\mathbf{L}\boldsymbol{k}^{C12})(NO_3)_3]$ ($\boldsymbol{k}$ = 12–14) to some specific variations in intermolecular interactions induced by the polycatenar effect? A previous detailed analysis of an exhaustive set of variable-temperature X-ray diffraction data collected for the hexacatenar complexes $[Ln(\mathbf{L14}^{C12})(NO_3)_3]$ (Ln = Pr–Gd) established that these solid complexes melted to give lamello-columnar mesophases around 100–120 °C, which were then transformed into cubic mesophases ($Im\bar{3}m$ space group) around 180 °C (Table 1).[19] We then attributed this rare sequence of phase transition to the existence of rodlike nitrato-bridged dimeric units $[Ln_2(\mathbf{L14}^{C12})_2(NO_3)_6]$ at room temperature, the shape of which was compatible with the formation of lamello-columnar mesophases. The entropically driven transformation of the latter rodlike dimers into disklike monomers $[Ln(\mathbf{L14}^{C12})(NO_3)_3]$ at higher temperatures were then responsible for the formation of the cubic organization in the subsequent mesophase.[19] This interpretation was supported by the crystal structures of the dimers $[Ln_2(\mathbf{L14}^{C0})_2(NO_3)_6]$ (Ln = Eu, Lu) observed in the solid state and by the solution behavior of $[Eu(\mathbf{L14}^{C12})(NO_3)_3]$, which exists as a mixture of monomer and dimer in noncoordinating CD_2Cl_2, see Equilibrium (4).[19]

Moreover, the analysis of variable-temperature (VT) ^1H NMR spectroscopic data by using van 't Hoff plots gave $\Delta H_{dim}^{Eu,\mathbf{L14}} = -25(2)\ kJ\,mol^{-1}$ and $\Delta S_{dim}^{Eu,\mathbf{L14}} = -47(5)\ J\,mol^{-1}\,K^{-1}$, in agreement with the trend expected for a simple dimerization process, which (i) is not strongly affected by solvation effects in this poorly coordinating solvent and (ii) produces the proposed entropically driven destruction of the dimer at high temperature [$\Delta S_{dim}^{Eu,\mathbf{L14}} < 0$

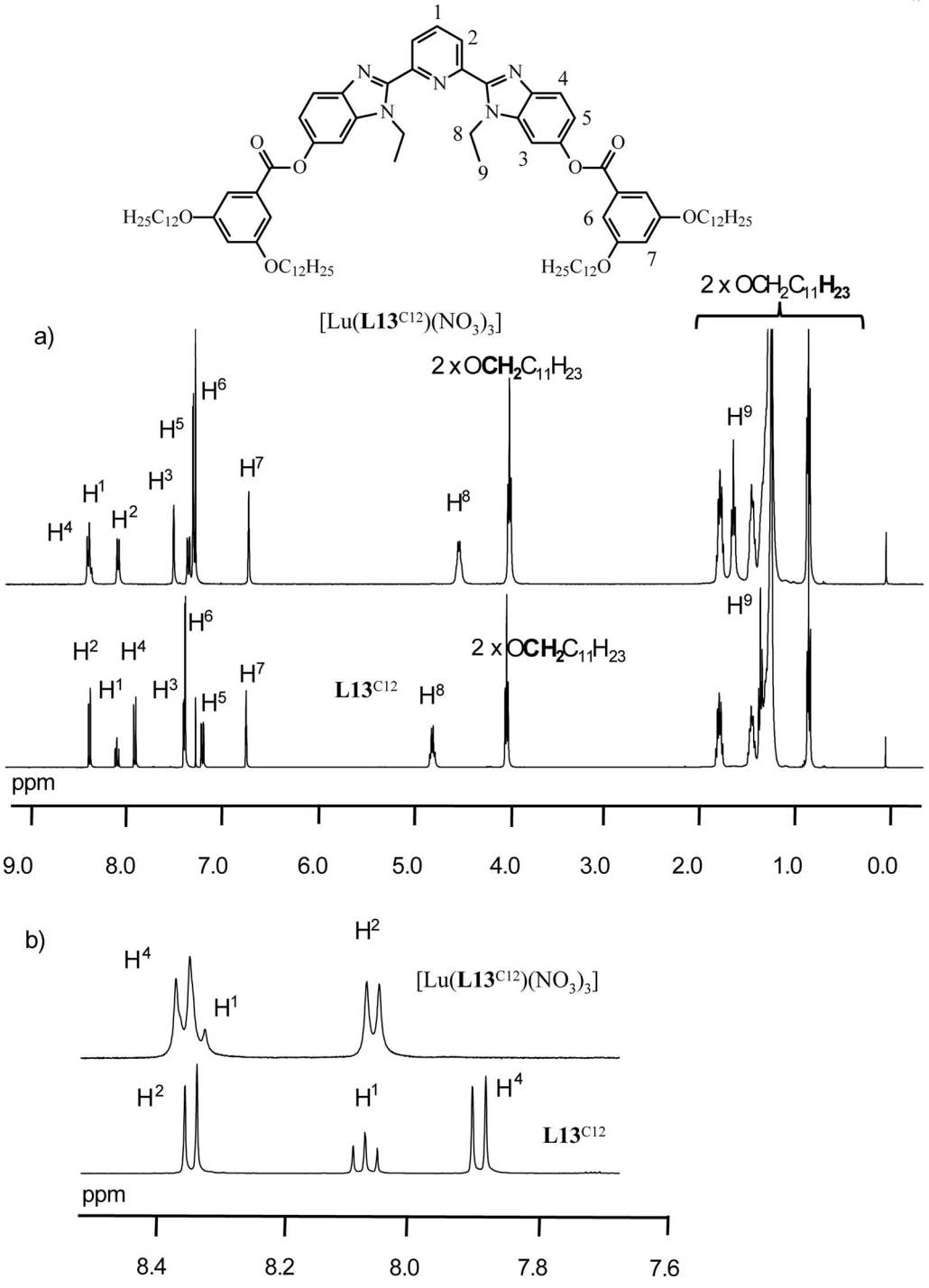

Figure 7. (a) ^{1}H NMR spectra of **L13**^{C12} and of its complex [Lu(**L13**^{C12})$(NO_3)_3$] with numbering scheme ($CDCl_3$, 298 K). (b) Highlight of the aromatic region.

and $T_{50\%} = \Delta H_{dim}^{Eu,\mathbf{L14}}/(\Delta S_{dim}^{Eu,\mathbf{L14}} + R\ln C_{tot}) = 293$ K whereby $T_{50\%}$ is the critical temperature at which the monomer represents 50% of the ligand distribution in CD_2Cl_2 ($C_{tot} = 0.01$ M)].[19] Altogether, the results and interpretation collected in ref.[19] suggested that the study of the dimerization process in noncoordinating organic solvents could be considered to be a model for the potential intercomplex interactions operating in the mesophases and controlling both phase transitions and organizations.[19] To check the validity of this approach, we repeated the same experiment shown in Equilibrium (4), but in $CDCl_3$, and we obtained completely different thermodynamic parameters for Equilibrium (4) (Table 2), together with a partial decomplexation of the ligand at millimolar concentrations, which allowed the estimation of the formation constants $\beta_{1,1}^{Eu,\mathbf{L14}}$ [Equilibrium (5)] and $\beta_{2,2}^{Eu,\mathbf{L14}}$ [Equilibrium (6)], and their thermodynamic characteristics by VT ^{1}H NMR spectroscopy (Table 2).[24]

Table 1. Phase-transition temperatures and enthalpy and entropy changes for ligands **L12**^{C12}–**L14**^{C12} and their complexes [Ln(**L*k***^{C12})$(NO_3)_3$] (***k*** = 12–14).

Compound	Transition[a]	T [°C]	ΔH [kJ mol^{-1}]	ΔS [J mol^{-1} K^{-1}]
L12^{C12}	Cr→I	172	47.7	108
[La(**L12**^{C12})$(NO_3)_3$]	Cr→Cr_1	–18	3.9	15
	Cr_1→Cr_2	84	1.9	5
	Cr_2→Cr_3	195	4.3	9
	Cr_3→Dec.	281	–	–
[Eu(**L12**^{C12})$(NO_3)_3$]	Cr→Cr_1	–20	1.1	4.3
	Cr_1→Cr_2	162	0.9	2.2
	Cr_2→Dec	260	–	–
[Lu(**L12**^{C12})$(NO_3)_3$]	Cr→Cr_1	–15	20.8	81
	Cr_1→Dec	247	–	–
[Y(**L12**^{C12})$(NO_3)_3$]	Cr→Cr_1	–19	0.6	2.4
	Cr_1→Dec.	255		
L13^{C12}	Cr→I	57	48.8	148
[La(**L13**^{C12})$(NO_3)_3$]	Cr→Cr_1	162	74.8	172
	Cr_1→Dec.	205	–	–
[Eu(**L13**^{C12})$(NO_3)_3$]	Cr→Cr_1	7	1.3	4.6
	Cr_1→Cr_2	51	1.4	4.3
	Cr_2→Dec.	207	–	–
[Lu(**L13**^{C12})$(NO_3)_3$]	Cr→Cr_1	–13	2.5	9.5
	Cr_1→Dec	218	–	–
[Y(**L13**^{C12})$(NO_3)_3$]	Cr→Cr_1	5	4.0	14.5
	Cr_1→Cr_2	55	12.5	38
	Cr_2→Cr_3	130	3.6	9
	Cr_3→Dec.	213	–	–
L14^{C12}	Cr→I	58	31.5	95
[Pr(**L14**^{C12})$(NO_3)_3$]	g→M	100[b]	–	–
	M→Cub	140[b]	–	–
	Cub→Dec.	190	–	–
[Nd(**L14**^{C12})$(NO_3)_3$]	g→M	120[b]	–	–
	M→Cub	160[b]	–	–
	Cub→Dec.	180	–	–
[Sm(**L14**^{C12})$(NO_3)_3$]	g→M	160[b]	–	–
	M→Cub	180[b]	–	–
	Cub→Dec.	190	–	–
[Eu(**L14**^{C12})$(NO_3)_3$]	g→M	120[b]	–	–
	M→Cub	180[b]	–	–
	Cub→Dec.	190	–	–
[Gd(**L14**^{C12})$(NO_3)_3$]	g→M	100[b]	–	–
	M→Cub	160[b]	–	–
	Cub→Dec.	190	–	–
[Tb(**L14**^{C12})$(NO_3)_3$]	g→Cub	160[b]	–	–
	Cub→Dec.	171	–	–
[Dy(**L14**^{C12})$(NO_3)_3$]	g→M	90[b]	–	–
	M→Dec.	180	–	–
[Ho(**L14**^{C12})$(NO_3)_3$]	g→Cub	160[b]	–	–
	Cub→Dec.	175	–	–
[Er(**L14**^{C12})$(NO_3)_3$]	g→Col_h	150[b]	–	–
	Col_h→Cub	180[b]	–	–
	Cub→Dec.	185	–	–
[Tm(**L14**^{C12})$(NO_3)_3$]	g→M	160[b]	–	–
	M→Dec.	180	–	–
[Yb(**L14**^{C12})$(NO_3)_3$]	g→Col_h	175[b]	–	–
	Col_h→Dec.	195	–	–
[Lu(**L14**^{C12})$(NO_3)_3$]	g→Col_h	155[b]	–	–
	Col_h→I	190	–	–
	I→Dec.	195	–	–

[a] Cr = crystal, Col_h = hexagonal columnar phase, Cub = cubic phase, g = glass, M = lamello-columnar phase, I = isotropic fluid, Dec. = decomposition. Transition temperatures were obtained by differential scanning calorimetry (DSC), polarized light microscopy (PLM), and small-angle X-ray diffraction (SA-XRD) measurements, and are given for the second heating processes; the liquid crystalline phases were identified from their optical textures and from SA-XRD studies. [b] Glassy or second-order phase transitions were determined by PLM and SA-XRD in ref.[19]

$$2\,[Eu(\mathbf{L14}^{C12})(NO_3)_3] \rightleftharpoons [Eu_2(\mathbf{L14}^{C12})_2(NO_3)_6] \quad K_{dim}^{Eu,L14} \quad (4)$$

Table 2. Enthalpies ($\Delta H^{Eu,\mathbf{L14}}$ in kJ mol^{-1}), entropies ($\Delta S^{Eu,\mathbf{L14}}$ in J mol^{-1} K^{-1}), and free-energy ($\Delta G^{Eu,\mathbf{L14}}$ in kJ mol^{-1}) changes, and stability constants for Equilibria (4)–(6) at 298 K.

Solvent	CD_2Cl_2[19]	$CDCl_3$[24]
$\Delta H_{dim}^{Eu,\mathbf{L14}}$	–25(2)	–5(2)
$\Delta S_{dim}^{Eu,\mathbf{L14}}$	–47(5)	–1(10)
$\Delta G_{dim}^{Eu,\mathbf{L14}}$	–11(3)	–4.7(3.6)
$\log(K_{dim}^{Eu,\mathbf{L14}})$	1.9(5)	0.8(6)
$\Delta H_{1,1}^{Eu,\mathbf{L14}}$	[a]	13(4)
$\Delta S_{1,1}^{Eu,\mathbf{L14}}$	[a]	109(15)
$\Delta G_{1,1}^{Eu,\mathbf{L14}}$	[a]	–19.4(6.0)
$\log(\beta_{1,1}^{Eu,\mathbf{L14}})$	[a]	3.4(1.0)
$\Delta H_{2,2}^{Eu,\mathbf{L14}}$	[a]	21(6)
$\Delta S_{2,2}^{Eu,\mathbf{L14}}$	[a]	218(26)
$\Delta G_{2,2}^{Eu,\mathbf{L14}}$	[a]	–44.0(9.8)
$\log(\beta_{2,2}^{Eu,\mathbf{L14}})$	[a]	7.7(1.7)

[a] Not accessible because no decomplexation is observed in the ^{1}H NMR spectra at millimolar concentration.

For the dimerization process in solution [Equilibrium (4)], both $|\Delta H_{dim}^{Eu,\mathbf{L14}}|$ and $|\Delta S_{dim}^{Eu,\mathbf{L14}}|$ concomitantly decrease on going from CD_2Cl_2 to $CDCl_3$, a phenomenon reminiscent of enthalpy/entropy compensation. Since the same final dimeric complexes are involved in the two solvents, the variation of the enthalpy and entropy changes strictly originates from the different solvation free energies of the partners shown in Equilibrium (4). A rapid inspection of Table 2 suggests that the more polar chloroform solvent[25] better solvates the polar lanthanide complexes following the natural decreasing order of polarity $[Eu(NO_3)_3]$ > $[Eu(\mathbf{L14}^{C12})(NO_3)_3]$ > $[Eu_2(\mathbf{L14}^{C12})_2(NO_3)_6]$, which obviously reduces $K_{1,1}^{Eu,\mathbf{L14}}$, $\beta_{1,1}^{Eu,\mathbf{L14}}$, and $\beta_{2,2}^{Eu,\mathbf{L14}}$ on going from CD_2Cl_2 to $CDCl_3$. This observation has considerable (and negative) consequences for the development of potential correlations between solution-based thermodynamics and our original interpretation of intermolecular interactions occurring in the mesophases, whereby no solvent molecule is present. Based on the latter experiments, dichloromethane should be preferred over chloroform for recording parameters that are amenable to being used in potentially rationalizing cohesion in thermotropic lanthanidomesogens,[6d,6e] but there is no fundamental justification for considering dichloromethane itself as an innocent solvent. The crucial effect of solvation in the formation of lanthanide complexes and related aggregates in chloroform is further confirmed by the enthalpic and entropic contributions measured for Equilibria (5) and (6) (Table 2), which imply entropically driven processes only compatible with the two-step desolvation model first introduced by Choppin.[26]

To confront this reasoning and the effect of solvation on the dimerization of the less lipophilic tetracatenar [Ln(**L13**^{C12})$(NO_3)_3$] and dicatenar [Lu(**L12**^{C12})$(NO_3)_3$] complexes with lanthanide cations of variable size (Ln = La, Eu, Lu), we systematically recorded ^{1}H NMR spectra for these complexes, together with their translational self-diffusion coefficients by using Diffusion-Ordered Spec-

$$\mathbf{L14}^{C12} + Eu(NO_3)_3 \rightleftharpoons [Eu(\mathbf{L14}^{C12})(NO_3)_3] \qquad \beta_{1,1}^{Eu,L14} \qquad (5)$$

$$2\,\mathbf{L14}^{C12} + 2\,Eu(NO_3)_3 \rightleftharpoons [Eu_2(\mathbf{L14}^{C12})_2(NO_3)_6] \qquad \beta_{2,2}^{Eu,L14} \qquad (6)$$

Table 3. Experimental translational self-diffusion coefficients (D_x) and ratios of molecular weights $(MM_C/MM_L)_{exp.}$ [Equation (11)] for $\mathbf{L12}^{C12}$, $\mathbf{L13}^{C12}$, $\mathbf{L14}^{C12}$, and their complexes $[Ln(\mathbf{L}k)(NO_3)_3]$ and $[Ln_2(\mathbf{L}k)_2(NO_3)_6]$ in $CDCl_3$ at 298 K (Ln = Eu, Lu).

Compounds	D_x [$m^2 s^{-1}$]	$(MM_C/MM_L)_{exp.}$	$MM_{calcd.}$ [$g mol^{-1}$]	$(MM_C/MM_L)_{calcd.}$
$\mathbf{L12}^{C12}$	$6.9(2)\times10^{-10}$	–	976.3	–
$[Lu_2(\mathbf{L12}^{C12})_2(NO_3)_6]$	$4.8(9)\times10^{-10}$	3.0(3)	2674.6	2.7
$\mathbf{L13}^{C12}$	$5.20(4)\times10^{-10}$	–	1344.9	–
$[Lu_2(\mathbf{L13}^{C12})_2(NO_3)_6]$	$4.1(1)\times10^{-10}$	2.04(4)	3411.8	2.5
$[Eu_2(\mathbf{L13}^{C12})_2(NO_3)_6]$	$3.7(1)\times10^{-10}$	2.78(5)	3365.8	2.5
$[Eu(\mathbf{L13}^{C12})(NO_3)_3]$	$4.8(2)\times10^{-10}$	1.27(8)	1682.9	1.3
$\mathbf{L14}^{C12}$	$4.45(1)\times10^{-10}$	–	1713.6	–
$[Lu_2(\mathbf{L14}^{C12})_2(NO_3)_6]$	$3.50(3)\times10^{-10}$	2.06(2)	4149.2	2.4
$[Eu_2(\mathbf{L14}^{C12})_2(NO_3)_6]$	$3.2(2)\times10^{-10}$	2.7(1)	4103.2	2.4
$[Eu(\mathbf{L14}^{C12})(NO_3)_3]$	$4.36(3)\times10^{-10}$	1.06(1)	2051.6	1.2

troscopY (DOSY-NMR) in $CDCl_3$ at 298 K (Figure 7, Table 3). According to the Stokes–Einstein equation[27] modified for microfrictional theory [Equation (7)],[28] the translational self-diffusion coefficient D_x is simply related to the hydrodynamic radius r_H^x (k is Boltzmann's constant, T is the temperature, η is the viscosity of the solvent, and r_{solv}^x/r_H^x is a correcting factor when the size of the particles approaches that of the solvent molecules).

$$D_x = \left(\frac{kT}{6\pi\eta r_H^x}\right)\left(1 + 0.695\left(r_{solv}/r_H^x\right)^{2.234}\right) \qquad (7)$$

For large particles such as $\mathbf{L12}^{C12}$–$\mathbf{L14}^{C12}$ and their complexes in chloroform, the correction factor $1 + 0.695(r_{solv}^x/r_H^x)^{2.234} \approx 1.0$, and the introduction of the hydrodynamic volume V_H^x [Equation (8)] into (7) gives (9), which is eventually transformed into Equation (10) when the density ρ_H^x of the particle is considered (MM_x is the molecular mass of the particle and $\rho_H^x = MM_x/N_A V_H^x$, in which N_A is the Avogadro constant).

$$V_H^x = \frac{4}{3}\pi\left(r_H^x\right)^3 \qquad (8)$$

$$D_x = \left(\frac{kT}{6\pi\eta}\right)\left(\frac{4\pi}{3V_H^x}\right)^{1/3} \qquad (9)$$

$$D_x = \left(\frac{kT}{6\pi\eta}\right)\left(\frac{4\pi\rho_H^x N_A}{3MM_x}\right)^{1/3} \qquad (10)$$

By taking the C_{2v}-symmetrical monomeric free ligand as a reference for which MM_L is well-defined in solution (Figure 7), the ratio of the diffusion coefficients D_L and D_C (L = ligand, C = complex), each modeled with Equation (10), leads to (11), which is adapted for the rough estimation of the molecular weights of globular chemical species in solution.[29]

$$\frac{MM_C}{MM_L} = \left(\frac{D_L}{D_C}\right)^3 \frac{\rho_H^C}{\rho_H^L} \qquad (11)$$

Only the lutetium complexes $[Lu(\mathbf{L}k^{C12})(NO_3)_3]$ are soluble enough in $CDCl_3$ for recording reliable ^1H NMR spectra with the three ligands $\mathbf{L12}^{C12}$, $\mathbf{L13}^{C12}$, and $\mathbf{L14}^{C12}$. For all complexes, a single species is detected in solution (Table S3 in the Supporting Information), in which (i) the C_{2v} symmetry of the ligand strand is retained (7 signals for aromatic protons, enantiotopic methylene protons, Figure 7), (ii) the deshielding of the pyridine protons is larger for H^1 than for H^2 (Figure 7), and (iii) NOE effects can be detected between H^2 and H^8. These features are diagnostic for the meridional *cis,cis* coordination of the tridentate binding unit to Lu^{III} as depicted in Scheme 1.[30] Reasonably assuming that the coordination of $Lu(NO_3)_3$ to the large lipophilic ligands $\mathbf{L12}^{C12}$, $\mathbf{L13}^{C12}$, or $\mathbf{L14}^{C12}$ has only a minor effect on their hydrodynamic densities (i.e., $\rho_H^C/\rho_H^L \approx 1$), the introduction of the diffusion coefficients measured for the free and complexed ligands into Equation (11) gives MM_C/MM_L ratios that demonstrate the exclusive formation of dimers $[Lu_2(\mathbf{L}k^{C12})_2(NO_3)_6]$ in chloroform (Table 3). For Ln = Eu, the complex with $\mathbf{L12}^{C12}$ is poorly soluble and escapes reliable investigation by ^1H NMR spectroscopy, but the observation of resolved signals for the free ligand together with two different complexes in the ^1H NMR spectrum of $[Eu(\mathbf{L13}^{C12})(NO_3)_3]$ mirrors the partial decomplexation processes previously established for $[Eu(\mathbf{L14}^{C12})(NO_3)_3]$ and modeled with Equilibria (4), (5), and (6).[19] In both systems ($\mathbf{L13}^{C12}$and $\mathbf{L14}^{C12}$), the self-diffusion coefficients confirm the coexistence of monomers $[Eu(\mathbf{L}k^{C12})(NO_3)_3]$ and dimers $[Eu_2(\mathbf{L}k^{C12})_2(NO_3)_6]$, in line with Equilibrium (4) and with previous discussions (Table 3). Finally,

for Ln = La, chemical exchanges operating at an intermediate rate on the NMR spectroscopic timescale at 298 K produce ^{1}H NMR spectra that are too broad to be addressed. We conclude that the dimerization process, which implies intermolecular cohesion between the complexes, exists along the second part of the lanthanide series for Ln/**L*k*** = 1 ratio (Ln = Eu–Lu) with dicatenar (**L12**^{C12}), tetracatenar (**L13**^{C12}), and hexacatenar (**L14**^{C12}) ligands in $CDCl_3$. Surprisingly, this process is favored on going from Ln = Eu to Ln = Lu in $CDCl_3$, thus leading to pure dimer with Ln = Lu, whereas the opposite trend and the formation of pure monomer has been previously reported in CD_2Cl_2 for [Lu(**L14**^{C12})$(NO_3)_3$].[19] This result again highlights the drastic influence of solvation on the dimerization of complexes in solution, which prevents valuable correlations between the solution-based thermodynamic parameters of cohesion with those operating in pure mesophases. Moreover, such considerable solvation effects are not restricted to the dimerization process [Equilibrium (4)], but they also affect the formation constants of the complexes and their speciation in solution. For instance, the spectrophotometric titrations of **L12**^{C12}, **L13**^{C12}, or **L14**^{C12} with Ln$(NO_3)_3$·$x$$H_2O$ (Ln = La, Eu, Lu) performed in CH_2Cl_2/CH_3CN (3:1) indeed show the formation of two absorbing complexes (established by factor analyses[31] and confirmed by the lack of isosbestic points, Figure 8). Nonlinear least-squares fits[32]

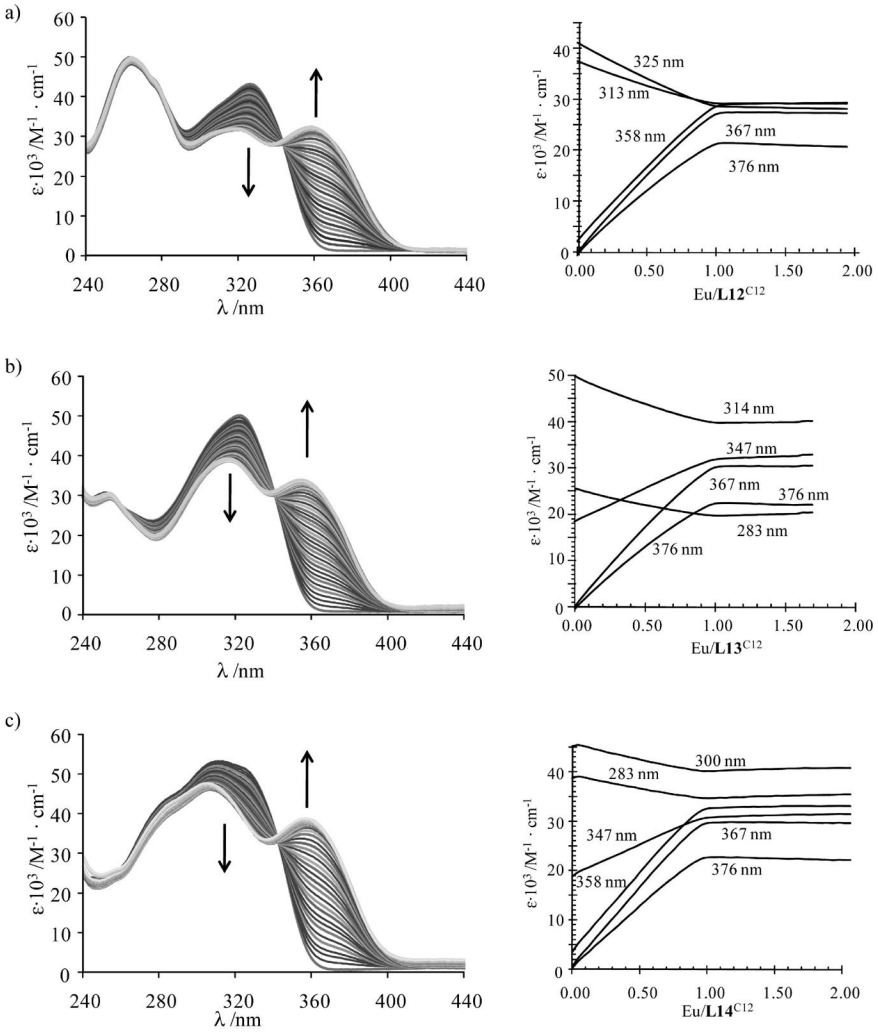

Figure 8. Variation of absorption spectra and corresponding variation of observed molar extinctions at five different wavelengths observed during the spectrophotometric titrations of (a) **L12**^{C12}, (b) **L13**^{C12}, and (c) **L14**^{C12} with Eu$(NO_3)_3$·$3H_2O$ [2×10^{-4} M in CH_2Cl_2/CH_3CN (3:1) at 298 K].

$$2\,\mathbf{L}k^{C12} + 2\,Ln(NO_3)_3 \rightleftharpoons [Ln_2(\mathbf{L}k^{C12})_2(NO_3)_6] \quad \beta_{2,2}^{Ln,Lk} \qquad (12)$$

$$3\,\mathbf{L}k^{C12} + 2\,Ln(NO_3)_3 \rightleftharpoons [Ln_2(\mathbf{L}k^{C12})_3(NO_3)_6] \quad \beta_{2,3}^{Ln,Lk} \qquad (13)$$

converge to Equilibria (12) and (13) and give thermodynamic formation constants, which do not depend, within experimental errors, on the number of alkoxy chains attached to the central tridentate binding unit (Table 4).

Table 4. Experimental thermodynamic formation constants $\log(\beta_{2,2}^{Ln,\mathbf{L}k})$ and $\log(\beta_{2,3}^{Ln,\mathbf{L}k})$ for the complexes $[Ln_2(\mathbf{L}k^{C12})_2(NO_3)_6]$ and $[Ln_2(\mathbf{L}k^{C12})_3(NO_3)_6]$ in CH_2Cl_2/CH_3CN (3:1) at 298 K (Ln = La, Eu, Lu; k = 12–14).

Ln^{III}	La	Eu	Lu
$\log(\beta_{2,2}^{Ln,\mathbf{L12}^{C12}})$	19.0(5)	17.9(4)	19.3(6)
$\log(\beta_{2,3}^{Ln,\mathbf{L12}^{C12}})$	23.8(6)	22.4(6)	24.1(8)
$\log(\beta_{2,2}^{Ln,\mathbf{L13}^{C12}})$	17.8(3)	17.6(4)	19.1(6)
$\log(\beta_{2,3}^{Ln,\mathbf{L13}^{C12}})$	22.1(4)	22.2(5)	23.9(7)
$\log(\beta_{2,2}^{Ln,\mathbf{L14}^{C12}})$	19.2(5)	17.4(5)	18.4(7)
$\log(\beta_{2,3}^{Ln,\mathbf{L14}^{C12}})$	23.7(6)	22.6(6)	24.5(9)

It is worth stressing here that $\log(\beta_{2,2}^{Eu,\mathbf{L14}})$ = 17.4(5) measured in CH_2Cl_2/CH_3CN (3:1, Table 4) is ten orders of magnitude larger than its value estimated by NMR spectroscopy in $CDCl_3$ [$\log(\beta_{2,2}^{Eu,\mathbf{L14}})$ = 7.7(1.7), Table 2], which eventually confirms the crucial solvation effects that control the formation of these lanthanide complexes. The detection of 2:3 nitrato complexes $[Ln_2(\mathbf{L}k^{C12})_3(NO_3)_6]$ in an excess amount of ligand is reminiscent of similar behaviors reported for $[La_2(2,2':6',2''\text{-terpyridine})_3(NO_3)_6]$[33] and $[Lu_2\{2,6\text{-bis}(N\text{-ethylbenzimidazol-2-yl})\text{pyridine}\}_3(SCN)_6]$,[24] which exist as ionic pairs $\{[Ln\mathbf{L}_2(NO_3)_2]^+[Ln\mathbf{L}(NO_3)_4]^-\}$.

Conclusion

After more than a decade of considerable efforts toward rationalizing the enthalpic and entropic origins of melting processes in thermotropic lanthanidomesogens, we are able to consider this field with a balanced opinion. On the positive side, there is no doubt that the two successive melting processes responsible for the formation and the subsequent destruction of thermotropic mesophases can be approached with some chemical intuition relying on the potential well depths (enthalpy) and force constants (entropy) of intermolecular interactions, which are modified during phase transitions. Assuming that simple microsegregation processes are the crucial driving force for the organization of amphiphilic molecules in the solid state, the stepwise increase of the flexible chain lengths corresponds to a special situation for which enthalpy/entropy compensation prevails, thus leading to an approximate invariance of the melting temperatures. However, the connection of several diverging flexible chains onto the rigid polarizable core induces significant deviations from enthalpy/entropy compensation, which empirically produce lower melting temperatures due to an increase in entropy incompletely balanced by some parallel increase in enthalpy. According to the basic Equations (2) and (3) that model weak intermolecular interactions,[13] we deduce that the increased intermolecular cohesion on going from di- to tetra-, hexa-, and finally to dodecacatenar ligands and their lanthanide complexes are characterized by an increase in force constant (tighter correlation between methylene units), which is less than compensated by a deeper well depth (more interacting methylene units). Following these deductions, we nevertheless succeeded in tuning melting temperatures, thereby leading to (i) the formation of the first cubic lanthanide-containing mesophase in 2005[19] and (ii) the design of the lanthanidomesogen that displays the lowest reported melting temperature in 2007.[20] However, this tentative rational approach proved to be limited in its demonstration, and therefore in its acceptance by the scientific liquid-crystal community, because of the difficulty in obtaining reliable thermodynamic parameters for highly lipophilic polycatenars such as $\mathbf{L12}^{C12}$–$\mathbf{L14}^{C12}$, or dendrimeric systems,[6e,19] which usually exhibit glassy or second-order phase transitions. Moreover, our attempt to collect alternative, but complementary thermodynamic information for the dimerization of lipophilic complexes in solution [Equilibrium (4)] as a model for intercomplex interactions operating in mesophases also failed because of the crucial role played by solvation, even in poorly coordinating organic solvents.

Experimental Section

General: Chemicals were purchased from Fluka AG and Aldrich, and used without further purification unless otherwise stated. The syntheses of the ligands $\mathbf{L12}^{C12}$,[24] $\mathbf{L13}^{C12}$[19], and $\mathbf{L14}^{C12}$[19] are described in the Supporting Information (Scheme S1). The complexes $[Ln(\mathbf{L14}^{C12})(NO_3)_3]$ (Ln = Pr–Lu, except Pm) were prepared according to a literature procedure.[19] The nitrate salts $Ln(NO_3)_3{\cdot}xH_2O$ were prepared from the corresponding oxide (Aldrich, 99.99%).[34] The Ln content of the solid salt was determined by complexometric titrations with Titriplex III (Merck) in the presence of urotropine and xylene orange.[35] Acetonitrile and dichloromethane were distilled from calcium hydride. Silica gel plates Merck 60 F_{254} were used for thin-layer chromatography (TLC) and Fluka silica gel 60 (0.04–0.063 mm) or Acros neutral activated alumina (0.050–0.200 mm) was used for preparative column chromatography.

Preparation of the Complexes $[Ln(\mathbf{L}k^{C12})(NO_3)_3]$ (k = 12–13; Ln = La, Eu, Lu and Y): $Ln(NO_3)_3{\cdot}xH_2O$ (Ln = La, Eu, Lu, Y, x = 1–3; 62 μmol, 1 equiv.) in acetonitrile (5 mL) was added to a solution (5 mL) of $\mathbf{L}k^{C12}$ (k = 12 or 13; 62 μmol, 1 equiv.) in dichloromethane. The resulting clear solutions were stirred for 1 h, concentrated, and cooled to –30 °C for 12 h. The insoluble white powders were collected by filtration and dried in vacuo to give $[Ln_2(\mathbf{L}k^{C12})(NO_3)_3]$ in 53–76% yields (Table S1 in the Supporting Information).

Spectroscopic Measurements: Spectrophotometric titrations were performed with a J&M diode array spectrometer (Tidas series) connected to an external computer. In a typical experiment, the ligand (50 mL) in CH_2Cl_2/CH_3CN (3:1, 10^{-4} M) was titrated at 298 K with a solution of $Ln(NO_3)_3{\cdot}xH_2O$ (10^{-3} M) in CH_2Cl_2/CH_3CN (3:1) under an inert atmosphere. After each addition of 0.20 mL, the absorbance was recorded with Hellma optrodes (optical path length 0.1 cm) immersed in the thermostatted titration vessel and connected to the spectrometer. Mathematical treatment of the spectrophotometric titrations was performed with factor analysis[31] and with the SPECFIT program.[32] ^1H and ^{13}C NMR spectra were recorded at 298 K with a Bruker Avance 400 MHz spectrometer. Chemical shifts are given in ppm with respect to TMS. Diffusion experiments (DOSY-NMR) were carried out at 400 MHz Larmor

frequency (293 K, $|complex|_{tot} = 5 \times 10^{-3}$ M). The complexes were prepared in situ and left to equilibrate for 48 h (CD_3CN, 293 K, $|complex|_{tot} = 5 \times 10^{-3}$ m). The pulse sequence used was the Bruker pulse program ledbpgp2s[36] which employs stimulated echo, bipolar gradients, and a longitudinal eddy current delay as the *z* filter. The four 2 ms gradient pulses have sine-bell shapes and amplitudes ranging linearly from 2.5 to 50 G cm^{-1} in 32 steps. The diffusion delay was in the range 60–140 ms depending on the analyte diffusion coefficient, and the number of scans was 32. The processing was done using a line broadening of 5 Hz and the diffusion coefficients were calculated with the Bruker processing package. DSC traces were obtained with Seiko DSC 220C and Mettler Toledo DSC1 Star Systems differential scanning calorimeters from 3–5 mg samples (5 °C min^{-1}, under N_2). The characterization of the mesophases were performed with a Leitz Orthoplan-Pol polarizing microscope with a Leitz LL 20×/0.40 polarizing objective, and equipped with a Linkam THMS 600 variable-temperature stage. The SAXS patterns were obtained with four different experimental setups, and in all cases, the crude powder was filled in Lindemann capillaries of 1 mm diameter. Diffraction patterns (laboratory source) were measured with a STOE transmission powder diffractometer system STADI P using a focused monochromatic Cu-$K_{\alpha 1}$ beam obtained from a curved Germanium monochromator (Johann-type) and collected on a curved image plate position-sensitive detector (IP-PSD). A calibration with silicon and copper laurate standards, for high and low angle domains, respectively, was preliminarily performed. Sample capillaries were placed in the high-temperature attachment for measurements in the range of desired temperatures (from –40 up to 170 °C) within ±0.05 °C. Periodicities up to 50 Å could be measured. The exposure times were varied from 1 to 4 h. Diffraction patterns (SLS) were alternatively measured using the synchrotron radiation Swiss Light Source (SLS) at the Paul Scherrer Institut (PSI), Villigen, Switzerland. Measurements were performed at the material science (MS) beamline using the wavelengths λ = 0.4328 or 0.87943 Å (depending on the sample). The microstrip detector, which covers an angular range of 60°, allows extremely fast in situ measurements depending on the temperature (around 50–80 s per temperature step), which prevents the decomposition of some fragile complexes under heating and gives reliable structural data to complete the DSC and polarized light microscopy (PLM) measurements. Moreover, the high signal/noise ratio allows the detection of weak Bragg peaks and leads to a more accurate indexation for some poorly organized phases. Elemental analyses were performed by Dr. H. Eder from the Microchemical Laboratory of the University of Geneva.

Supporting Information (see also the footnote on the first page of this article): Syntheses of ligands **L12**^{C12}, **L13**^{C12}, and **L14**^{C12} (Scheme S1) and their lanthanide complexes (Tables S1–S3).

Acknowledgments

We thank Ms. K.-L. Buchwalder, Ms. A. Rosset, and Ms. M. Wijttewaal for technical support. Financial support from the Swiss National Science Foundation is gratefully acknowledged.

[1] a) A. M. Giroud-Godquin, P. M. Maitlis, *Angew. Chem. Int. Ed. Engl.* **1991**, *30*, 375–402; b) D. W. Bruce, *J. Chem. Soc., Dalton Trans.* **1993**, 2983–2989; c) S. A. Hudson, P. M. Maitlis, *Chem. Rev.* **1993**, *93*, 861–885; d) J. L. Serrano, *Metallomesogens, Synthesis Properties and Applications*, VCH, Weinheim, **1996**; e) B. Donnio, D. W. Bruce, *Struct. Bonding (Berlin)* **1999**, *95*, 194–247; f) B. Donnio, D. Guillon, R. Deschenaux, D. W. Bruce, in: *Comprehensive Coordination Chemistry* (Eds.: J. A. McCleverty, T. J. Meyer), Elsevier, Oxford, UK, **2003**, vol. 7, ch. 79; g) R. W. Date, E. Fernandez Iglesias, K. E. Rowe, J. M. Elliott, D. W. Bruce, *Dalton Trans.* **2003**, 1914–1931.

[2] a) K. Binnemans, C. Görller-Walrand, *Chem. Rev.* **2002**, *102*, 2303–2346; b) E. Terazzi, S. Suarez, S. Torelli, H. Nozary, D. Imbert, O. Mamula, J.-P. Rivera, E. Guillet, J.-M. Bénech, G. Bernardinelli, R. Scopelliti, B. Donnio, D. Guillon, J.-C. G. Bünzli, C. Piguet, *Adv. Funct. Mater.* **2006**, *16*, 157–168; c) C. Piguet, J.-C. G. Bünzli, B. Donnio, D. Guillon, *Chem. Commun.* **2006**, 3755–3768.

[3] a) I. V. Ovchinnikov, Y. G. Galyametdinov, G. I. Ivanova, L. M. Yagfarova, *Dokl. Akad. Nauk SSSR* **1984**, *276*, 126–128; b) Y. G. Galyametdinov, I. V. Ovchinnikov, B. M. Bolotin, N. B. Etingen, G. I. Ivanova, L. M. Yagarova, *Izv. Akad. Nauk SSSR, Ser. Khim.* **1984**, 2379–2381; c) Y. G. Galyametdinov, D. Z. Zakieva, I. V. Ovchinnikov, *Izv. Akad. Nauk SSSR Ser. Khim.* **1986**, 491; d) I. V. Ovchinnikov, I. G. Galyametdinov, I. G. Bikchantaev, *Izv. Akad. Nauk SSSR Ser. Fiz.* **1989**, *53*, 1870–1879; e) R. M. Galimov, I. G. Bikchantaev, I. V. Ovchinnikov, *Zh. Strukt. Khim.* **1989**, *30*, 65–69; f) Y. G. Galyametdinov, M. A. Athanassopoulou, K. Griesar, O. Kharitonova, E. A. Soto Bustamante, L. Tinchurina, I. V. Ovchinnikov, W. Haase, *Chem. Mater.* **1996**, *8*, 922–926; g) K. Binnemans, Y. G. Galyametdinov, S. R. Collinson, D. W. Bruce, *J. Mater. Chem.* **1998**, *8*, 1551–1553; h) K. Binnemans, Y. G. Galyametdinov, R. Van Deun, D. W. Bruce, S. R. Collinson, A. P. Polishchuk, I. Bikchantaev, W. Haase, A. V. Prosvirin, L. Tinchurina, U. Litvinov, A. Gubajdullin, A. Rakhmatullin, K. Uytterhoeven, L. Van Meervelt, *J. Am. Chem. Soc.* **2000**, *122*, 4335–4344; i) R. van Deun, K. Binnemans, *Liq. Cryst.* **2001**, *28*, 621–627; j) Y. G. Galyametdinov, W. Haase, L. Malykhina, A. Prosvirin, I. Bikchantaev, A. Rakhmatullin, K. Binnemans, *Chem. Eur. J.* **2001**, *7*, 99–105; k) K. Binnemans, D. Moors, T. N. Parac-Vogt, R. van Deun, D. Hinz-Hübner, G. Meyer, *Liq. Cryst.* **2002**, *29*, 1209–1216; l) N. V. Rao, M. K. Paul, T. R. Rao, A. Prasad, *Liq. Cryst.* **2002**, *29*, 1243–1246; m) L. Van Meervelt, K. Uytterhoeven, R. van Deun, K. Binnemans, *Z. Kristallogr. NCS* **2003**, *218*, 488–490.

[4] a) C. Piechocki, J. Simon, J. J. André, D. Guillon, P. Petit, A. Skoulios, P. Weber, *Chem. Phys. Lett.* **1985**, *122*, 124–128; b) T. Komatsu, K. Ohta, T. Fujimoto, I. Yamamoto, *J. Mater. Chem.* **1994**, *4*, 533–536; c) T. Toupance, P. Bassoul, L. Mineau, J. Simon, *J. Phys. Chem.* **1996**, *100*, 11704–11710; d) H. Miwa, N. Kobayashi, K. Ban, K. Ohta, *Bull. Chem. Soc. Jpn.* **1999**, *72*, 2719–2728; e) K. Ban, K. Nishizawa, K. Ohta, A. van de Craats, J. M. Warman, I. Yamamoto, H. Shirai, *J. Mater. Chem.* **2001**, *11*, 321–331; f) J. Sleven, C. Görller-Walrand, K. Binnemans, *Mater. Sci. Eng. C* **2001**, *C18*, 229–238; g) F. Maeda, K. Hatsusaka, K. Ohta, M. Kimura, *J. Mater. Chem.* **2003**, *13*, 243–251; h) K. Binnemans, J. Sleven, S. De Feyter, F. C. De Schryver, B. Donnio, D. Guillon, *Chem. Mater.* **2003**, *15*, 3930–3938.

[5] a) F. Martin, S. R. Collinson, D. W. Bruce, *Liq. Cryst.* **2000**, *27*, 859–863; b) S. Clark, J. M. Elliot, J. R. Chipperfield, P. M. Styring, E. Sinn, *Inorg. Chem. Commun.* **2002**, *5*, 249–251; c) J. M. Elliott, J. R. Chipperfield, S. Clark, S. J. Teat, E. Sinn, *Inorg. Chem.* **2002**, *41*, 293–299; d) J. L. Sessler, W. B. Callaway, S. P. Dudek, R. W. Date, D. W. Bruce, *Inorg. Chem.* **2004**, *43*, 6650–6653; e) I. Aiello, M. Ghedini, A. Grisolia, D. Pucci, O. Francescangeli, *Liq. Cryst.* **2005**, *32*, 763–769; f) T. Cardinaels, J. Ramaekers, D. Guillon, B. Donnio, K. Binnemans, *J. Am. Chem. Soc.* **2005**, *127*, 17602–17603; g) T. Cardinaels, K. Driesen, T. N. Parac-Vogt, B. Heinrich, C. Bourgogne, D. Guillon, B. Donnio, K. Binnemans, *Chem. Mater.* **2005**, *17*, 6589–6598; h) J. L. Sessler, P. J. Melfi, E. Tomat, W. Callaway, M. T. Huggins, P. L. Gordon, K. D. Webster, R. W. Date, D. W. Bruce, B. Donnio, *J. Alloys Compd.* **2006**, *418*, 171–177; i) K. Binnemans, K. Lodewyckx, T. Cardinaels, T. N. Parac-Vogt, C. Bourgogne, D. Guillon, B. Donnio, *Eur. J. Inorg. Chem.* **2006**,

150–157; j) T. Cardinaels, J. Ramaekers, P. Nockemann, K. Driesen, K. Van Hecke, L. Van Meervelt, S. Lei, S. De Feyter, D. Guillon, B. Donnio, K. Binnemans, *Chem. Mater.* **2008**, *20*, 1278–1291.

[6] a) B. Donnio, D. Guillon, *Adv. Polym. Sci.* **2006**, *201*, 45–155; b) R. Deschenaux, B. Donnio, D. Guillon, *New J. Chem.* **2007**, *31*, 1064–1073; c) B. Donnio, S. Buathong, I. Bury, D. Guillon, *Chem. Soc. Rev.* **2007**, *36*, 1495–1513; d) E. Terazzi, B. Bocquet, S. Campidelli, B. Donnio, D. Guillon, R. Deschenaux, C. Piguet, *Chem. Commun.* **2006**, 2922–2924; e) T. B. Jensen, E. Terazzi, B. Donnio, D. Guillon, C. Piguet, *Chem. Commun.* **2008**, 181–183.

[7] a) B. Donnio, K. E. Rowe, C. P. Roll, D. W. Bruce, *Mol. Cryst. Liq. Cryst.* **1999**, *332*, 383–390; b) D. Guillon, *Struct. Bonding (Berlin)* **1999**, *95*, 41–82; c) D. W. Bruce, *Acc. Chem. Res.* **2000**, *33*, 831–840; d) C. Tschierske, *J. Mater. Chem.* **2001**, *11*, 2647–2671; e) J.-F. Eckert, U. Maciejczuk, D. Guillon, J.-F. Nierengarten, *Chem. Commun.* **2001**, 1278–1279; f) M. Ogura, H. Miyoshi, S. P. Naik, T. Okubo, *J. Am. Chem. Soc.* **2004**, *126*, 10937–10944; g) T. Cardinaels, K. Driesen, T. N. Parac-Vogt, B. Heinrich, C. Bourgogne, D. Guillon, B. Donnio, K. Binnemans, *Chem. Mater.* **2005**, *17*, 6589–6598; h) C. Tschierske, *Chem. Soc. Rev.* **2007**, *36*, 1930–1970.

[8] C. T. Imrie, P. A. Henderson, *Chem. Soc. Rev.* **2007**, *36*, 2096–2124.

[9] a) D. Guillon, A. Skoulios, *J. Phys.* **1976**, *37*, 797–800; b) A. Skoulios, D. Guillon, *Mol. Cryst. Liq. Cryst.* **1988**, *165*, 317–332.

[10] H. Nozary, C. Piguet, P. Tissot, G. Bernardinelli, J.-C. G. Bünzli, R. Deschenaux, D. Guillon, *J. Am. Chem. Soc.* **1998**, *120*, 12274–12288.

[11] a) M. S. Searle, D. H. Williams, *J. Am. Chem. Soc.* **1992**, *114*, 10690–10697; b) M. S. Searle, M. S. Westwell, D. H. Williams, *J. Chem. Soc. Perkin Trans. 2* **1995**, 141–151; c) D. H. Williams, D. P. O'Brien, B. Bardsley, *J. Am. Chem. Soc.* **2001**, *123*, 737–738.

[12] A. A. Levchenko, C. K. Yee, A. N. Parikh, A. Navrotsky, *Chem. Mater.* **2005**, *17*, 5428–5438.

[13] D. M. Ford, *J. Am. Chem. Soc.* **2005**, *127*, 16167–16170.

[14] a) P. W. Atkins, *Physical Chemistry*, 5th ed., Oxford University Press, Oxford, **1994**, p. 773; b) G. Karlström, B. Jönsson, *Intermolecular Interactions*, **2005**, http://www.teokem.lu.se/.

[15] a) C. A. Hunter, J. K. M. Sanders, *J. Am. Chem. Soc.* **1990**, *112*, 5525–5534; b) C. A. Hunter, *Chem. Soc. Rev.* **1994**, *23*, 101–109; c) S. J. Cantrill, A. R. Pease, J. F. Stoddart, *J. Chem. Soc., Dalton Trans.* **2000**, 3715–3734; d) S. L. Cockroft, C. A. Hunter, K. R. Lawson, J. Perkins, C. J. Urch, *J. Am. Chem. Soc.* **2005**, *127*, 8594–8595; e) S. L. Cockroft, J. Perkins, C. Zonta, H. Adams, S. E. Spey, C. M. R. Low, J. G. Vinter, K. R. Lawson, C. J. Urch, C. A. Hunter, *Org. Biomol. Chem.* **2007**, *5*, 1062–1080; f) S. Grimme, *Angew. Chem. Int. Ed.* **2008**, *47*, 3430–3434; g) J. K. Klosterman, Y. Yamauchi, M. Fujita, *Chem. Soc. Rev.* **2009**, *38*, 1714–1725.

[16] K. E. Rowe, D. W. Bruce, *J. Mater. Chem.* **1998**, *8*, 331–341.

[17] H. Nozary, C. Piguet, J.-P. Rivera, P. Tissot, P.-Y. Morgantini, J. Weber, G. Bernardinelli, J.-C. G. Bünzli, R. Deschenaux, B. Donnio, D. Guillon, *Chem. Mater.* **2002**, *14*, 1075–1090.

[18] H. Nozary, C. Piguet, J.-P. Rivera, P. Tissot, G. Bernardinelli, N. Vulliermet, J. Weber, J.-C. G. Bünzli, *Inorg. Chem.* **2000**, *39*, 5286–5298.

[19] E. Terazzi, S. Torelli, G. Bernardinelli, J.-P. Rivera, J.-M. Bénech, C. Bourgogne, B. Donnio, D. Guillon, D. Imbert, J.-C. G. Bünzli, A. Pinto, D. Jeannerat, C. Piguet, *J. Am. Chem. Soc.* **2005**, *127*, 888–903.

[20] A. Escande, L. Guénée, H. Nozary, G. Bernardinelli, F. Gumy, A. Aebischer, J.-C. G. Bünzli, B. Donnio, D. Guillon, C. Piguet, *Chem. Eur. J.* **2007**, *13*, 8696–8713.

[21] E. Terazzi, L. Guénée, P.-Y. Morgantini, G. Bernardinelli, B. Donnio, D. Guillon, C. Piguet, *Chem. Eur. J.* **2007**, *13*, 1674–1691.

[22] a) J. P. Bedel, H. T. Nguyen, J. C. Rouillon, J. P. Marcerou, G. Sigaud, P. Barois, *Mol. Cryst. Liq. Cryst.* **1999**, *332*, 163–171; b) H. T. Nguyen, J. C. Rouillon, J. P. Marcerou, J. P. Bedel, P. Barois, S. Sarmento, *Mol. Cryst. Liq. Cryst.* **1999**, *328*, 177–184; c) J. P. Bedel, J. C. Rouillon, J. P. Marcerou, M. Laguerre, H. T. Nguyen, M. F. Achard, *Liq. Cryst.* **2000**, *27*, 1411–1421; d) J. P. Bedel, J. C. Rouillon, J. P. Marcerou, M. Laguerre, M. F. Achard, H. T. Nguyen, *Liq. Cryst.* **2000**, *27*, 103–113; e) J. P. Bedel, J. C. Rouillon, J. P. Marcerou, M. Laguerre, H. T. Nguyen, M. F. Achard, *Liq. Cryst.* **2001**, *28*, 1285–1292.

[23] ΔH_c and ΔS_c cannot be obtained by using standard differential scanning calorimetry (DSC) for [Lu(**L11**^{C12})$(NO_3)_3$], because the phase transition leading to the isotropic liquid is not of the first-order type, that is, that for which the heat capacity is close to infinitity at the transition temperature, $C_P = (\partial H/\partial T)_P \rightarrow \infty$. See: a) P. W. Atkins, *Physical Chemistry*, 5th ed., Oxford University Press, Oxford, **1994**, p. 200; b) G. J. M. Koper, C. B. Minkenberg, I. S. Upton, J. H. van Esch, E. J. R. Sudhölter, *J. Phys. Chem. B* **2009**, *113*, 15597–15601, for the definition and use of the Ehrenfest classification of phase transitions.

[24] A. Escande, L. Guénée, K.-L. Buchwalder, C. Piguet, *Inorg. Chem.* **2009**, *48*, 1132–1147.

[25] a) L. R. Snyder, *J. Chromatogr.* **1974**, *92*, 223–230; b) L. R. Snyder, *J. Chromatogr. Science* **1978**, *16*, 223–234.

[26] a) G. R. Choppin, in: *Lanthanide Probes in Life, Chemical and Earth Sciences* (Eds.: J.-C. G. Bünzli, G. R. Choppin), Elsevier, Amsterdam, **1989**, chapter 1; b) C. Piguet, J.-C. G. Bünzli, *Chem. Soc. Rev.* **1999**, *28*, 347–358; c) J.-C. G. Bünzli, C. Piguet, *Chem. Rev.* **2002**, *102*, 1897–1928.

[27] a) A. Einstein, *Ann. Phys.* **1906**, *19*, 289–306; b) A. Einstein, *Ann. Phys.* **1906**, *19*, 371–381; c) M. Sharma, S. Yashonath, *J. Phys. Chem. B* **2006**, *110*, 17207–17211.

[28] A. Macchioni, G. Ciancaleoni, C. Zuccaccia, D. Zuccaccia, *Chem. Soc. Rev.* **2008**, *37*, 479–489, and references cited therein.

[29] a) P. Stilbs, *Prog. NMR Spectrosc.* **1986**, *19*, 1–45; b) A.-R. Waldeck, P. W. Kuchel, A. J. Lennon, B. E. Chapman, *Prog. NMR Spectrosc.* **1997**, *30*, 39–68; c) P. S. Pregosin, E. Martinez-Viviente, P. G. A. Kumar, *Dalton Trans.* **2003**, 4007–4014; d) A. Pastor, E. Martinez-Viviente, *Coord. Chem. Rev.* **2008**, *252*, 2314–2345; e) D. Li, G. Kagan, R. Hopson, P. G. Williard, *J. Am. Chem. Soc.* **2009**, *131*, 5627–5634; f) S. Augé, P.-O. Schmit, C. A. Crutchfield, M. T. Islam, D. J. Harris, E. Durand, M. Clemancey, A.-A. Quoineaud, J.-M. Lancelin, Y. Prigent, F. Taulelle, M.-A. Delsuc, *J. Phys. Chem. B* **2009**, *113*, 1914–1918.

[30] a) C. Piguet, J.-C. G. Bünzli, G. Bernardinelli, C. G. Bochet, P. Froidevaux, *J. Chem. Soc., Dalton Trans.* **1995**, 83–97; b) C. Piguet, J.-C. G. Bünzli, G. Bernardinelli, G. Hopfgartner, S. Petoud, O. Schaad, *J. Am. Chem. Soc.* **1996**, *118*, 6681–6697.

[31] E. R. Malinowski, D. G. Howery, *Factor Analysis in Chemistry*, Wiley, New York, **1980**.

[32] a) H. Gampp, M. Maeder, C. J. Meyer, A. Zuberbühler, *Talanta* **1985**, *32*, 1133–1139; b) H. Gampp, M. Maeder, C. J. Meyer, A. Zuberbühler, *Talanta* **1986**, *33*, 943–951.

[33] M. Fréchette, C. Bensimon, *Inorg. Chem.* **1995**, *34*, 3520–3527.

[34] J. F. Desreux, in: *Lanthanide Probes in Life, Chemical and Earth Sciences* (Eds.: J.-C. G. Bünzli, G. R. Choppin), Elsevier, Amsterdam, **1989**, chapter 2.

[35] G. Schwarzenbach, *Complexometric Titrations*, Chapman & Hall, London, **1957** p. 8.

[36] D. Wu, A. Chen, C. S. Johnson Jr., *J. Magn. Reson. A* **1995**, *115*, 260–264.

Received: December 9, 2009
Published Online: May 11, 2010

